Use of Ultrasound Imaging to Map Propagating Action Potential Waves in the Heart

NF Otani[1], R Singh[1], FH Fenton[1], J Butcher[1], DW Infanger[1], A Neumann[1], S Luther[2], RL Davisson[1], RF Gilmour Jr[1]

[1]Cornell University, Ithaca, NY
[2]Max Plank Institute, Leipzig, Germany

Abstract

Presently, the nature of action potential propagation deep within myocardial tissue is unclear. As a result, a complete understanding of cardiac dynamics remains elusory. Here we present a technique using ultrasound and electromechanical modeling that has the potential to unlock this mystery. We also present information suggesting tension in the heart behaves as a long-range force incapable of being captured through only local observation of myocardial tissue deformation.

1. Introduction

The imaging of action potential propagation in the heart has largely been limited to the heart's surface for many decades. As a result, a fundamental understanding of the dynamics underlying numerous cardiac arrhythmias has been difficult. Studies of the heart's electrophysiology using electrocardiograms (ECG), electrical probes, optical mapping, and various other technologies have provided a wealth of valuable information describing the electrical state of the heart. However, as long as an image of action potential propagation deep within the walls of the heart eludes us, our understanding will remain incomplete. At the clinical and research level, this lack of information has not only prevented us from developing a complete understanding of cardiac spatial dynamics, but, as a result, therapeutic tools targeting various electrical anomalies of the heart have not been able to reach their full potential. It is no surprise that sudden cardiac death continues to be the number one cause of death in the industrialized world.

Our lack of a deep, panoramic view of action potential activity means that we cannot say with certainty that ventricular fibrillation (VF) is caused by multiple reentrant action potential waves, although of course it is strongly suspected. Even if VF is a manifestation of multiple waves, the nature of the dynamics of these waves remains controversial, with their induction and maintenance being attributed to either tissue heterogeneity [1] or steep electrical restitution [2], and their spatial patterning thought to be composed of either several rotating waves on equal dynamical footing [3], or one dominant "mother rotor" wave driving fibrillatory conduction [4]. The lack of clarity on these issues has greatly complicated the development of effective therapies for the prevention and treatment of several types of tachyarrhythmias, including VF.

In this paper, we describe the ability of ultrasound to see wave-induced tissue deformation at depth and its potential to image the propagation of action potentials deep within myocardial tissue via electromechanical modeling. We also present our finding that active tensions in the heart produce long-range effects, thus precluding the possibility that deformations at a given location can be used as a marker for the presence of action potential activity at that location.

2. Experimental Methods

For *ex vivo* optical mapping of canine left ventricle myocardium, we used a method established previously (e.g., [5]). Briefly, an adult beagle was anesthetized and its heart was excised rapidly and placed in cool Tyrode solution. The circumflex coronary artery was cannulated and a transmural section of tissue from the lateral left ventricle measuring 50 by 50 mm was excised. The preparation was then perfused and superfused with 37.0°C normal Tyrode solution. Following equilibration, the preparation was stained with the voltage-sensitive dye Di-4-ANEPPS (10 μM).

Optical mapping imaging was conducted using excitation light provided by 16 high performance light emitting diodes (Luxeon III star, LXHL-FM3C, wavelength 530 ± 20 nm). The illumination efficiency was significantly enhanced by collimator lenses (Luxeon, LXHL-NX05). The fluorescence emission light was collected by a Navitar lens (DO-2595, focal length 25

mm, F/# 0.95), passed through a long-pass filter (<610 nm), and imaged by a 128 x 128 back-illuminated EMCDD array (electron-multiplied charge coupled device, Photometrics Cascade 128+). The signal was digitized with a 16bit A/D converter at frame rate of 500 Hz (full frame, 128 x 128 pixels). Motion artifact was reduced using affine image registration.

Simultaneously, ultrasound imaging was performed using a Vevo 770 high resolution imaging system (VisualSonics, Toronto, Canada). Images were acquired in B-mode using a single-element mechanical probe (RMV 704, focal length 12.7 mm, F/# 2.1) with broadband frequency of 30 MHz. The probe was coupled to the myocardial preparation using warmed Aquasonic 100 transmission gel (Parker Labs, Fairfield, NJ) providing images of a plane parallel to the surface imaged via optical mapping. Retrospective ultrasound cineloops were then synchronized in time with the optical mapping data and converted into tissue deformations using the Sum Absolute Difference method (SAD).

3. Mathematical Methods

To empirically relate deformation to stress, we started with the following equations:

$$\frac{\partial}{\partial X_N}\left[\frac{\partial T_{MN}(E)}{\partial E_{PQ}}\frac{\partial x_P}{\partial X_Q}+T_{MN}^{active}-pC_{NM}^{-1}\right]=0 \qquad (1)$$

and

$$\det(F)=1 \qquad (2)$$

Here X_N and x_p (N,p=1,2,3), are the coordinates in the undeformed and deformed coordinate systems, respectively, $T_{MN}(E)$ is the passive second Piola-Kirchhoff stress tensor, which depends on the strain tensor E, p is the local hydrostatic pressure, $F_{jM}=\partial x_j/\partial X_M$ is the deformation gradient tensor, C = F^TF, and T_{NM}^{active} is the active stress tensor due to the action potential induced force generated parallel to the orientation of the myocardial fibers. Sums over repeated indices are implicit. Equation (1) is a statement of force balance and ignores inertia, a standard assumption for the timescales we are considering [6]. It also assumes the myocardium is an elastic medium. While the myocardium is perhaps better described as pseudoelastic, the variations of the stretch ratios (strains) for any given stress are no more than 20% [7], so we find this simplification appropriate for our study. Equation (2) together with the appearance of the hydrostatic pressure in Eq. (1) expresses the assumption of incompressibility, a common assumption in the study of cardiac biomechanics [8-10].

For the purposes of this paper, we used the linearized version of these equations,

$$\frac{\partial}{\partial X_N}\left[\frac{1}{2}\frac{\partial T_{NM}}{\partial E_{PQ}}(0)\left(\frac{\partial \delta x_P}{\partial X_Q}+\frac{\partial \delta x_Q}{\partial X_P}\right)+T_{NM}^{active}-p\delta_{NM}\right]=0 \qquad (3)$$

and

$$\partial \delta x_M/\partial X_M=0 \qquad (4)$$

where T_{NM}^{active}, p, and the displacements ($\delta x_P = x_P - X_P$) are all assumed small. In the case of ventricular fibrillation or in any situation where tissue deformations are typically small, this approximation should hold. Futhermore, for these preliminary studies, we used the simple form $\partial T_{MN}/\partial E_{PQ}(0)=\delta_{MP}\delta_{NQ}$ for the elasticity of the tissue.

Eqs. (4) and (5) were the fundamental equations used to develop our forward model and inverse model. The principal reason for building the forward model was to generate deformation data with which to test the main algorithm, the "inverse" model. These two models were simulated using a three dimensional finite element code applied to a cube with 10 nodes in each spatial direction, and solved via matrix inversion in the least square sense with a hat weighting function for the displacements and a unit weighting function for the pressure and active tension. In the forward model, all three vector components of the displacement for each node (1000 nodes) and a pressure for each element (729 elements) were solved for, given the active tensions associated with a propagating action potential wave. In the inverse model, the pressure, one component of the displacement, and the active tension, assumed only nonzero in the local fiber direction, were solved for given the remaining two components of the displacement.

4. Results

A propagating action potential, measured using optical mapping, and its induced deformation field in the tissue, measured using ultrasound, are presented in Figure 1. The right panels show the progressive movement of the action potential across the tissue from left to right. Noting that red and yellow corresponds to the regions where the membrane is depolarized, one can clearly see demarcations of the wave front (right panel, top) and wave back (right panel, bottom). For the same instances in time, the left panels depict the corresponding action potential induced deformations of the tissue in terms of displacement vectors, with the color representing the magnitude of displacement. We observe that, as the action potential travels by, the displacement vectors reorient themselves and increase in magnitude (changing in color from blue-green to red-yellow in Fig. 1, left panels).

Our computational study suggests that these

displacement vectors can be used to reconstruct the active stresses associated with the action potential. As shown in Fig. 2, the inverse model is capable of reproducing the active stress field (Fig. 2(c)) associated with the deformations (Fig. 2(b)) produced by a propagating action potential (Fig. 2(a)). This example shows how 3-D ultrasound data might be handled; more conventional 2-D ultrasound data can also be used with our method assuming variation of the action potential profile through the imaging plane is small. We have found that plane wave action potential propagation can be approximately reproduced with this assumption (not shown).

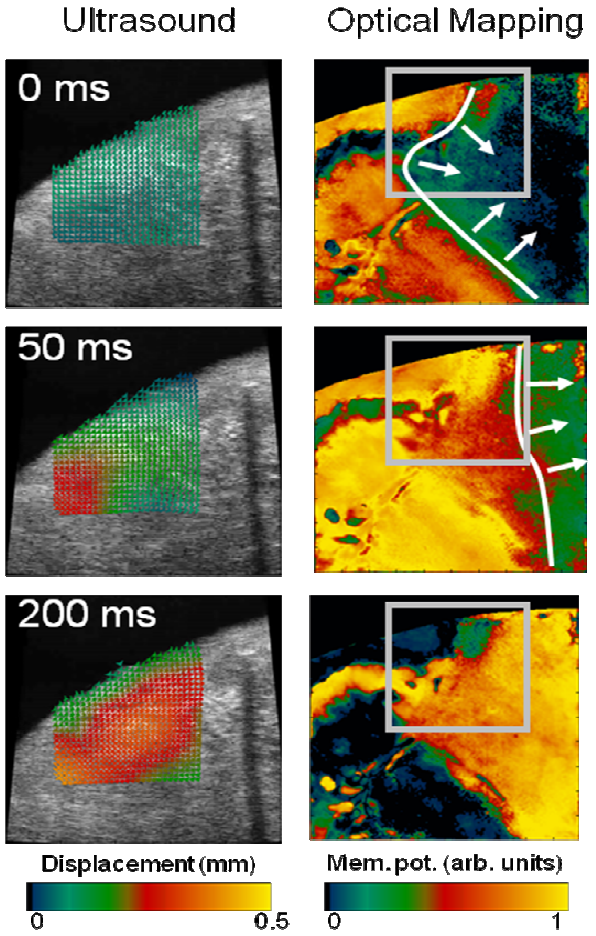

Figure 1. A series of three ultrasound images and calculated tissue displacements (top panels) and three optical mapping images (bottom panels) of approximately the same region during the passage of the same action potential. Red and yellow correspond to depolarization. Field of view in the upper panels: approximate 1.5 cm x 1.5 cm; lower panels: approximately 3 cm x 3 cm.

In order to better understand the nature of tissue deformation in response to localized stresses, such as those generated by propagating action potentials, we used Eqs. (4) and (5) to derive, in closed form, the displacements and pressures resulting from active tension applied at a single point. This was achieved by rewriting Eqs. (4) and (5) in cylindrical coordinates (Z, R, and φ) about the point, assuming axisymmetry in the φ direction and isotropy in the passive tension. The active tension was defined as,

$$T_{ZZ}(R,Z) = \frac{t_0\sqrt{2\pi}}{R}\delta(R)\delta(Z) \qquad (5)$$

with all other components equaling zero, where t_0 is the magnitude of the active stress in the Z direction and δ is the Dirac delta function. The solutions could then simplified by converting them to spherical coordinates ($\Re$,φ,θ):

$$\delta Z(\Re,\theta) = \frac{\pi t_0}{2T}\frac{1}{\Re^2}\cos\theta\left(1-3\cos^2\theta\right) \qquad (6)$$

$$\delta R(\Re,\theta) = \frac{\pi t_0}{2T}\frac{1}{\Re^2}\sin\theta\left(1-3\cos^2\theta\right) \qquad (7)$$

$$p(\Re,\theta) = \frac{\pi t_0}{\Re^3}\left(1-3\cos^2\theta\right) \qquad (8)$$

where $T \equiv \partial T_{MN}(0)/\partial E_{PQ}$ is the linear elasticity.

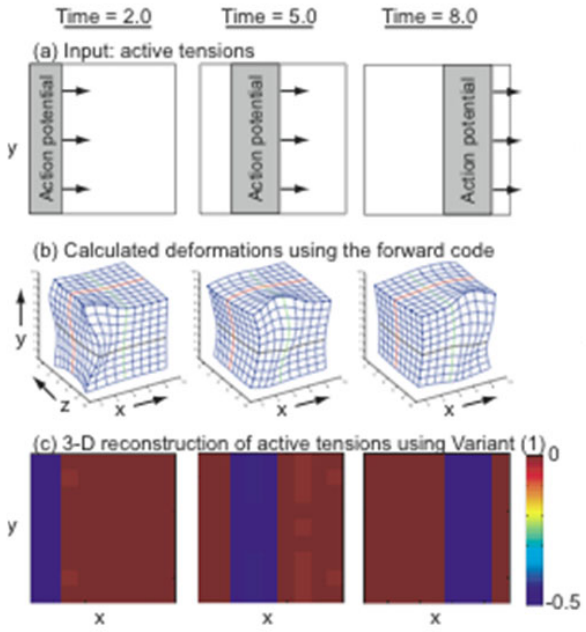

Figure 2. (a) Applied active tension in the local fiber direction as a function of time and space. Tension = - 0.5, in the gray regions, and zero everywhere else. (b) Resulting deformations of the cubically shaped tissue system, as calculated by the forward model. (c) Reconstruction of the active tensions in the local fiber direction, as calculated by the inverse model. Length and time scales in this figure are arbitrary, as the calculation at each time determines a separate global equilibrium, and the equation itself has no characteristic length scales.

These Green's function solutions for Eqs. (4) and (5) show that the displacements in the cylindrical coordinates Z and R fall off as $1/\Re^2$ in the spherical radial direction while the pressure decreases as $1/\Re^3$. The active tension thus behaves like a long-range force, affecting the displacements and pressure far from the actual source. We note that the displacements increase linearly with the active tension and inversely with the elasticity of the tissue. However, the pressure, which enforces the incompressibility condition, is directly proportional to the active tension but independent of the elastic properties of the tissue.

5. Discussion and conclusions

This paper presents a method for viewing action potential propagation at depth in the heart using ultrasound imaging and electromechanical modeling. Ultrasound has the ability to capture tissue deformations at depth both noninvasively and at very high temporal and spatial resolutions. The method consists of employing an inverse model that translates the deformations observed in B-mode ultrasound into action-potential induced active stresses. Although we did not validate this capability using experimental data, we were able to demonstrate proof-of-concept for a simulated data set developed using a forward model.

We also demonstrate that active tensions convey their effects over long distances in the myocardium. This eliminates the possibility that a technique can simply use the local presence of deformation as a marker for the presence of action potentials activity nearby. That is, since the deformation anywhere in the heart can be carried over long distances, it is not possible to determine the location of the source, the action potential or active stresses, without considering the entire problem, including boundary conditions, under the framework of an electromechanical model.

Other groups have worked in using echocardiography to capture action potential induced "electromechanical waves" [11]. These waves correspond to the fast time-scale shear waves produced by an action potential and yield valuable information on the mechanical state of the heart. However, since the detection of these waves requires very high temporal resolutions, only capable currently through gating techniques, they cannot be used to study unstable arrhythmias.

The technique we propose here is still rudimentary as the models used in this study are far from realistic. In order to improve our electromechanical model, we must consider nonlinearity of the tissue response and realistic constitutive laws defining the passive response of our tissue. Indeed, our electromechanical model *in vivo* will need to have more sophisticated boundary conditions. However, these problems are not insurmountable; we believe solutions can eventually be incorporated into our proposed technique to yield insight into action potential propagation at greater depths than is currently possible.

Acknowledgements

We would like to thank the American Heart Association (Grant #0830384N) and the National Science Foundation (Grant #0800793 and #0926190) for ongoing support.

References

[1] Sampson KJ, Henriquez C. Simulation and prediction of functional block in the presence of structural and ionic heterogeneity. *Am J Physiol*. 2001;281:H2597-H2603.

[2] Gilmour RF, Jr., Chialvo DR. Electrical restitution, critical mass, and the riddle of fibrillation. *J Cardiovasc Electrophysiol*. 1999;10:1087-9.

[3] Moe GK. On the multiple wavelet hypothesis of atrial fibrillation. *Arch Int Pharmacodyn Ther*. 1962;140:183–188.

[4] Chen J, Mandapati R, Berenfeld O, Skanes AC, Jalife J, High-frequency periodic sources underlie ventricular fibrillation in the isolated rabbit heart, Circ Res. 2000 Jan 7-21;86(1):86-93.

[5] Riccio ML, Koller ML, Gilmour RF, Jr. Electrical restitution and spatiotemporal organization during ventricular fibrillation. *Circ Res*. 1999;84:955-63.

[6] Whiteley JP, Bishop MJ, Gavaghan DJ, Soft tissue modeling of cardiac fibres for use in coupled mechano-electric simulations, Bulletin of Mathematical Biology, 2007;69:2199-2225.

[7] Demer LL, Yin FCP, Passive biaxial mechanical properties of isolated canine myocardium, J Physiol, 1983;339:615-630.

[8] Costa KD, Holmes JW, McCulloch AD, Modelling cardiac mechanical properties in three dimensions, Philos Trans Roy Soc Lond, 2001;A35:1233-1250.

[9] Guccione JM, McCulloch AD, and Waldman LK, Passive material properties of intact ventricular myocardium determined from a cylindrical model, ASME J Biomech Engng, 1991;113:42-55.

[10] Nash MP, Hunter PJ, Computational Mechanics of the heart, J Elasticity, 2000;61:113-141.

[11]Pernot M, Fujikura K, Fung-Kee-Fung SD, Konofagou EE, ECG-gated, mechanical and electromechanical wave imaging of cardiovascular tissues in vivo, Ultrasound Med Biol, 2007;33(7):1075–1085.

Address for correspondence:
Niels F. Otani
T7-008B Veterinary Research Tower
Cornell University, Ithaca, NY 14850
Email: nfo1@cornell.edu